Hydrogen gas sensor based on mesoporous In_2O_3 with fast response/recovery and ppb level detection limit

Zhijie Li[1*], Shengnan Yan[1], Zhonglin Wu[1], Hao Li[1], Junqiang Wang[1], Wenzhong Shen[2], Zhiguo Wang[1], YongQing Fu[3*]

[1]School of Physics, University of Electronic Science and Technology of China, Chengdu, 610054, P. R. China

[2]State Key Laboratory of Coal Conversion, Institute of Coal Chemistry, Chinese Academy of Science, Taiyuan, 030001, China

[3]Faculty of Engineering and Environment, Northumbria University, Newcastle Upon Tyne, NE1 8ST, UK

Corresponding Authors

*E-mail: zhijieli@uestc.edu.cn (Zhijie Li).

*E-mail: Richard.fu@northumbria.ac.uk (Richard YongQing Fu).

Abstract

Hydrogen gas sensors were fabricated using mesoporous In_2O_3 synthesized using hydrothermal reaction and calcination processes. Their best performance for the hydrogen detection was found at a working temperature of 260 ^oC with a high response of 18.0 toward 500 ppm hydrogen, fast response/recovery times (e.g. 1.7 s/1.5 s for 500 ppm hydrogen), and a low detection limit down to 10 ppb. Using air as the carrier gas, the mesoporous In_2O_3 sensors exhibited good reversibility and repeatability towards hydrogen gas. They also showed a good selectivity for hydrogen compared to other commonly investigated gases including NH_3, CO, ethyl alcohol, ethyl acetate, styrene, CH_2Cl_2 and formaldehyde. In addition, the sensors showed good long-term stability. The good sensing performance of these hydrogen sensors is attributed to the formation of mesoporous structures, large specific surface areas and numerous chemisorbed oxygen ions on the surfaces of the mesoporous In_2O_3.

Keywords*:* In_2O_3; Mesoporous structure; Hydrothermal; Hydrogen; Gas sensor

1. Introduction

Hydrogen gas is widely utilized in ammonia production, petroleum refining, metallurgical industry and fine organic synthesis. It is colorless and odorless, but is extremely flammable and explosive in air. Therefore, detection of traces of hydrogen gas is essential to mitigate the danger of explosion caused by leaks of hydrogen during its production, storage, transportation and usage. To achieve highly efficient real-time monitoring capability, hydrogen gas sensors must have rapid response/recovery, high sensitivity, good selectivity and low detection limits. In particular, the fast response/recovery is critical for early warning of hazardous hydrogen leaks in air.

Over the past decades, various types of hydrogen gas sensors have been developed, including semiconductor [1, 2], thermoelectrics [3, 4] optical [5-8] and surface acoustic wave [9, 10] sensors. Among them, the semiconductor sensors are simple, inexpensive, highly sensitive, and can be easily integrated with microelectronic devices. Many different types of semiconducting metal oxides have been investigated in the literature as potential materials for fabricating hydrogen gas sensors. These are summarized in Table 1, and mainly include WO_3[11-14], ZnO [15-18], NiO [19-21], SnO_2 [22-24], TiO_2 [25, 26], MoO_3 [27, 28], CuO [29], MgO [30] and In_2O_3 [31, 32]. The sensing mechanisms of these sensors are based mainly on chemical reactions between hydrogen with the negatively charged oxygen species on the surfaces of metal oxide sensing materials [33]. Oxygen molecules in air are easily absorbed on the surfaces of metal oxides to form different chemisorbed oxygen species, such are O_2^- ions when the working temperature is below 100 ^oC or O^- ions when above 100 ^oC. These reactions can be listed as below [34, 35]:

$$O_{2(gas)} \leftrightarrow O_{2(ads)} \quad (1)$$

$$O_{2(ads)} + e^- \rightarrow O_2^-{}_{(ads)} \quad (< 100\ ^oC) \quad (2)$$

$$O_2^-{}_{(ads)} + e^- \rightarrow 2O^-{}_{(ads)} \quad (100\ ^oC \sim 300\ ^oC) \quad (3)$$

When the metal oxides are exposed to hydrogen, the hydrogen molecules will react with those chemisorbed oxygen species to form H_2O, thus releasing electrons as

summarized in the chemical reactions of (4) or (5) at a working temperature either blow or above 100 ºC [36], respectively. These processes will cause decreases of the resistance of the gas sensors.

$$2H_2 + O_2^-{}_{(ads)} = 2H_2O + e^- \quad (< 100\ ^oC) \tag{4}$$

$$H_2 + O^-{}_{(ads)} = H_2O + e^- \quad (100\ ^oC \sim 300\ ^oC) \tag{5}$$

Table 1 Hydrogen sensing properties of gas sensors based on different semiconducting metal oxides reported in literature.

Materials and structures	Working Temp.(ºC)	C_{H2} (ppm)	Response	Response/ recovery time	Detection Limit	Ref.
WO_3 thin films	200	1000	9 [a]	60s/80s	-	[11]
WO_3 nanosheets	250	1%	80% [b]	120s/235s	-	[12]
WO_3 nanotube	450	500	17.6 [a]	25s/-	10 ppm	[13]
WO_3 thin films	300	3600	1.32 [a]	12s/40s	-	[14]
ZnO nanorods	180	500	264% [b]	127s/203s	-	[15]
ZnO nanorods	150	10000	77% [b]	10s/116s	-	[16]
ZnO nanorods	100	10000	67% [b]	14s/100s	-	[17]
ZnO nanorod array	250	1000	1370% [b]	20s/25s	-	[18]
NiO nanostructure	150	1000	119.63% [b]	6s/0.5s	30 ppm	[19]
NiO nanowires	300	1000	91% [b]	88s/39s	50 ppm	[20]
NiO thin film	175	1000	46.3 [a]	81s/322s	-	[21]
SnO_2 thin film	300	250	28 [a]	15s/4s	100 ppm	[22]
SnO_2 nanofibers	150	10000	2.4 [a]	21s/33s	600 ppm	[23]
Honeycombed	340	1	8.4 [a]	4s/10s	0.05 ppm	[24]
p-TiO_2 thin film	150	1000	28.5% [b]	2.4s/34.6s	-	[25]
TiO_2 thin film	225	10000	8100 [a]	120s/420s	-	[26]
a-MoO_3 nanowires	260	15000	0.85[c]	3.0s/2.7s	100 ppm	[27]
CuO NW networks	300	100	340 [a]	60s/2s	-	[29]
MgO nanocube	200	5000	25.4 [a]	140 s/130 s	-	[30]
In_2O_3 flower-like	210	100	1.4 [a]	11s/12s	10 ppm	[31]
In_2O_3 nanowires	200	500	0.1 [c]	31s/80s	500 ppm	[32]

Note: [a]: R_{air}/R_{H2}; [b]: $100(R_{air}-R_{H2})/R_{H2}$; [c]: $(R_{air}-R_{H2})/R_{H2}$

Decrease of the electrical resistance of sensors is corresponding to the change of hydrogen concentration. As summarized in Table 1, there are many types of hydrogen gas sensors based on various semiconducting metal oxides. Some of them have fast response/recovery rates for hydrogen sensing, such as those based on a-MoO_3 nanowires [27] and p-TiO_2 thin film [25], but their response values are low and their detection limits are normally higher than ppm level. Although high response values to hydrogen have been achieved in those sensors made of certain types of metal oxides including TiO_2 thin film [26], CuO nanowire network [29] and NiO thin film [21], their response/recovery speeds were reported to be quite low. Therefore, many of these hydrogen sensing materials have been further modified by adding/doping with noble metal nanoparticles or metal ions to enhance their sensing properties [37-40], especially for improving their response/recovery speeds. However, this will complicate the preparation processes of materials and devices, thus resulting in increased cost and complexity. Currently it is critically required for single-phase metal oxide based hydrogen gas sensors with high sensitivity, fast response/recovery, high selectivity and low level detection limit.

In_2O_3 is one of the important n-type semiconductor metal oxides with good catalytic performance. Good sensing properties have been reported using In_2O_3 nanostructures to detect NO_2 [41], H_2S [42], CO [43], ethyl alcohol [44], formaldehyde [45], and hydrogen. For example, Chen et al [31] reported that flower-like In_2O_3 nanostructures prepared using a hydrothermal method showed a response of 1.4 (R_{air}/R_{H2}) to 100 ppm hydrogen with response/recovery time of 11 s/12 s and a detection limit of 10 ppm at 210 ^oC. Qurashi et al [32] prepared In_2O_3 nanowires on silicon using a chemical vapor deposition method, and then used them to fabricate hydrogen sensors which showed a response of 0.1 ($(R_{air}-R_{H2})/R_{H2}$) for 500 ppm hydrogen at 200 ^oC, with response/recovery times of 31 s/80 s and a detection limit of 500 ppm. However, for these reported In_2O_3 based hydrogen gas sensors, the response values were very low, and the detection limits were all above ppm level. Therefore, In_2O_3 based hydrogen gas sensors with fast response/recovery, high response and low level detection limit are urgently needed. The mesoporous In_2O_3 has

large-scale and highly active surface areas, which are beneficial to the sensing performance for hydrogen detection. Especially, the mesoporous structure facilitates fast adsorption and desorption of hydrogen molecules, which is beneficial to enhanced response and recovery speeds of gas sensors. However, the mesoporous In_2O_3 has never been reported to be used for hydrogen gas sensors.

In this paper, mesoporous In_2O_3 with large surface areas and highly active surfaces was prepared using hydrothermal reaction and calcination processes. The hydrogen gas sensor based on the mesoporous In_2O_3 showed high sensitivity, fast response and recovery, and detection limit of ppb level.

2. Experimental procedures

2.1 Synthesis and characterization of mesoporous In_2O_3 structures

Mesoporous In_2O_3 was prepared using hydrothermal reaction and calcination processes. In a typical synthesis process, $In(NO_3)_3$ of 3 g was dissolved into 60 ml of HNO_3 solution (0.01 mol/L), and then 15 ml of $NH_3 \cdot H_2O$ (13 mol/L) was added into the above solution at 50 ^oC and magnetically stirred for 30 min to form a homogeneous sol. This homogeneous sol was added into a 100 ml Teflon-lined stainless steel autoclave and hydrothermally reacted for 10 hrs at 150 ^oC in an electric oven. After cooled down to room temperature in air, the white precipitate in the autoclave was collected and washed using distilled water for three times, and was dried at 80 ^oC in air for 6 hrs to obtain the white indium hydroxide. Finally, the indium hydroxide was heat-treated at 500 ^oC for 2 hrs in air to obtain the yellow colored indium oxide.

Scanning electron microscope (SEM, InspectF50) was used to observe surface morphology of the samples. High-resolution transmission electron microscope (HRTEM JEM-2200FS) and selected area electron diffraction (SAED) were used for the microstructure analysis. X-ray diffraction (XRD) analysis was conducted to study the crystalline structure of samples using Rigaku D/max-2500 X-ray diffractometer with Cu Kα radiation. Diffuse reflectance spectra (DRS) of the powders were obtained to check the band-gaps of samples using a UV-2101 Shimadzu apparatus

with $BaSO_4$ as a reference. X-ray photoelectron spectroscope (XPS, Kratos Axis-Ultra DLD with Mg Ka radiation) was used to study the chemical binding of In_2O_3. The nitrogen adsorption-desorption isotherms were obtained using a nitrogen physisorption apparatus of Autosorb iQ Station operated at 77.35 K. Before N_2 gas physisorption, the sample was outgassed at 300 °C for 12 hrs in a vacuum chamber. The specific surface area of In_2O_3 and pore diameter distribution were calculated using Brunauer−Emmett−Teller (BET) method and density functional theory (DFT), respectively. The total pore volumes (V_{total}) were obtained using the adsorption amount at P/P_0 of 0.99.

2.3 Fabrication and measurement of gas sensor

The sensor was made on an alumina ceramic tube with a Ni-Cr heating resistor to control the working temperature, and the detailed description of the testing setup has been reported before [46]. The sensing material of In_2O_3 was dispersed in ethanol and dip-coated onto the surface of alumina ceramic tube to form a sensing layer. They were then heat-treated at 200 ^oC for 2 hrs. The gas sensor was placed in a tightly sealed box (with a volume of 2 liters). The testing gas (hydrogen in this case) was injected into the testing chamber using a precision micro-injector. The hydrogen gas concentrations were adjusted by injecting different volumes of diluted hydrogen into the chamber. Changes of the sensor's electrical resistance were continuously recorded per second using a source meter (Keithley 2400), with a data reading rate of 1700 per second through GPIB at 4½ digits. The gas response of the sensor is defined as the ratio between the sensor's resistance in air (Ra) and that in the hydrogen (Rg). The relative humidity was maintained at 40% in all the testing processes.

3. Results and discussion

3.1 Structural and morphological characteristics of mesoporous In_2O_3

XRD pattern of the as-prepared precursor after the hydrothermal reaction is shown in Fig. 1. All the diffraction peaks can be indexed to cubic crystal structure of $In(OH)_3$ (JCPDS Card No. 16-0161). Fig. 1 also shows the XRD pattern of the heat-treated

sample, and all the diffraction peaks are in good agreements with the standard cubic structure of In_2O_3 crystallite (JCPDS Card No. 06-0416) with the lattice parameters of a=b=c=10.118 Å. No other characteristic peaks were observed, indicating that the $In(OH)_3$ precursor was completely transformed into crystalline In_2O_3 after the heat treatment at 500 ^oC. Using the Scherrer equation [44], the average crystallite size of In_2O_3 was calculated to be 29.6 nm.

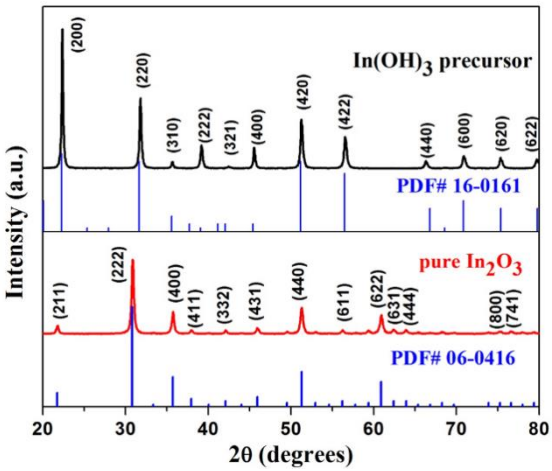

Fig. 1 XRD spectra of the $In(OH)_3$ precursor and the sample of In_2O_3.

SEM images of the In_2O_3 film on the alumina ceramic tube are shown in Figs. 2a and 2b, which reveal that the In_2O_3 samples are composed of spherical nanoparticles and have smooth and uniform surface but with highly porous structures on the alumina ceramic tube. TEM image in Fig. 2c also shows the average diameter of In_2O_3 nanoparticles is about 30 nm, which agrees with the diameter of In_2O_3 crystals calculated from the XRD analysis. In addition, many mesoporous structures with sizes from 5 nm to 20 nm can be found in these nanoparticles. Fig. 2d shows the HRTEM lattice image of the In_2O_3. The obtained lattice fringes and the corresponding SAED pattern (shown in Fig. 2c) indicate a good crystallinity. The measured lattice fringe spacings of 0.293 nm and 0.253 nm (in Fig. 2d) are corresponding to the crystal planes of (222) and (400) of cubic In_2O_3 [47], respectively.

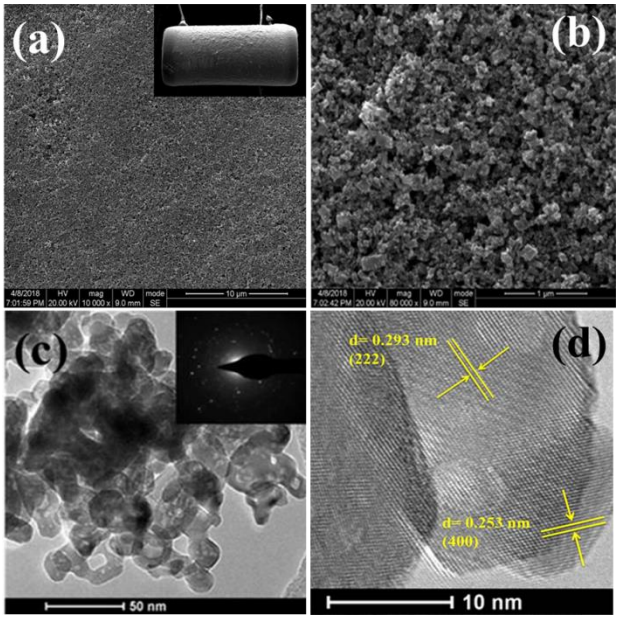

Fig. 2 (a) and (b) SEM images of mesoporous In_2O_3 film on alumina ceramic tube; (c) TEM and (d) HRTEM images of mesoporous In_2O_3. (The inset in 2a is SEM image of the sensor and the inset in 2c is the SAED pattern)

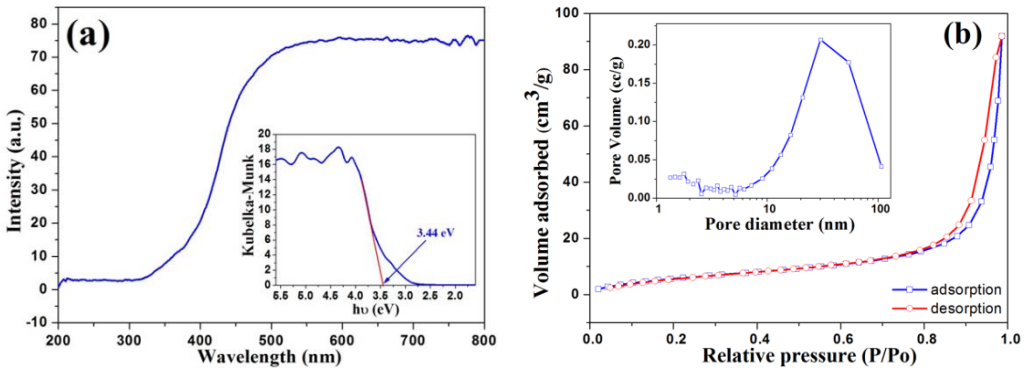

Fig. 3. (a) DRS spectrum of mesoporous In_2O_3 (the inset is the band gap spectrum). (b) N_2 adsorption/desorption isotherm of mesoporous In_2O_3 (the inset is pore size distributions).

The diffuse reflectance spectrum of mesoporous In_2O_3 is shown in Fig. 3a. In order to calculate its optical band-gap (Eg), the wavelength values were changed into photon energy values as shown in the inset of Fig. 3a, and the reflectance values, *R*, were translated into absorbance values using the Kubelka-Munk function, e.g., equation (6) [48]:

$$F(R) = \frac{(1-R)^2}{2R} \quad (6)$$

Where *F(R)* is the Kubelka-Munk function and *R* is the reflectance value. The optical band-gap (Eg) can be calculated by extrapolating the linear section of the curve to F(*R*) = 0 (see the inset of Fig. 3a as an example). The obtained optical band-gap (Eg) of the mesoporous In_2O_3 based on the DRS curve is 3.44 eV. It is slightly less than the reported band-gap of 3.6 eV for the In_2O_3 [49, 50].

Fig. 3b shows the N_2 adsorption/desorption isotherm and the calculated pore size distributions of the In_2O_3. The adsorption/desorption isotherm with a hysteresis loop clearly reveals its mesoporous structure [51]. The pore size of In_2O_3 is centered at a value of 31 nm, indicating that there are not only mesoporous structures inside the particles, but also many mesopores due to the accumulation of the In_2O_3 nanoparticles. The calculated pore volume of the In_2O_3 sample obtained from the DFT method is 0.142 cm^3/g, and the specific surface area from the BET method is 23.5 m^2/g. The mesoporous structures and large specific surface areas are beneficial for the absorption/desorption of the tested gas molecules, which could contribute to the fast response/recovery and high sensitivity in hydrogen detection [49, 50].

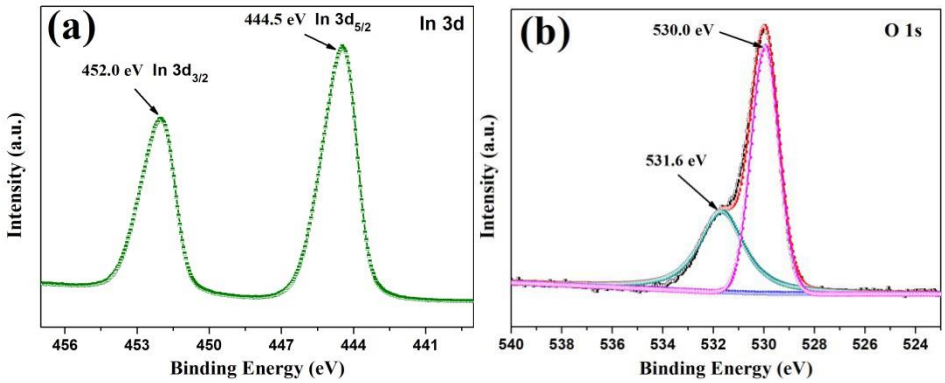

Fig. 4. (a) In 3d and (b) O 1s of XPS spectra of mesoporous In_2O_3

Fig. 4 shows XPS spectra of In 3d and O 1s of mesoporous In_2O_3. In Fig. 4a, both peaks at the binding energies of 452.0 and 444.5 eV are corresponding to the characteristic ones of In $3d_{3/2}$ and In $3d_{5/2}$ [52], which is in a good agreement with the chemical valence of In^{3+} ions. The O 1s XPS spectrum of the mesoporous In_2O_3 in Fig. 4b shows two deconvoluted peaks at 530.0 eV and 531.6 eV, respectively. The peak centered at 530.0 eV is corresponding to the lattice oxygen in In_2O_3 crystals, and the other one centered at 531.6 eV is attributed to the chemisorbed oxygen

species on the surfaces of mesoporous In_2O_3 [53]. By analyzing the integral areas at 530.0 eV and 531.6 eV, the atomic ratio of the lattice oxygen and chemisorbed oxygen species at the sample surface can be estimated and the ratio is 58.1:41.9. This indicates that there are lots of chemisorbed oxygen species on the surfaces of the In_2O_3, which could increase the sensitivity of the mesoporous In_2O_3 based sensors.

3.2 Gas sensing properties of mesoporous In_2O_3 based gas sensor

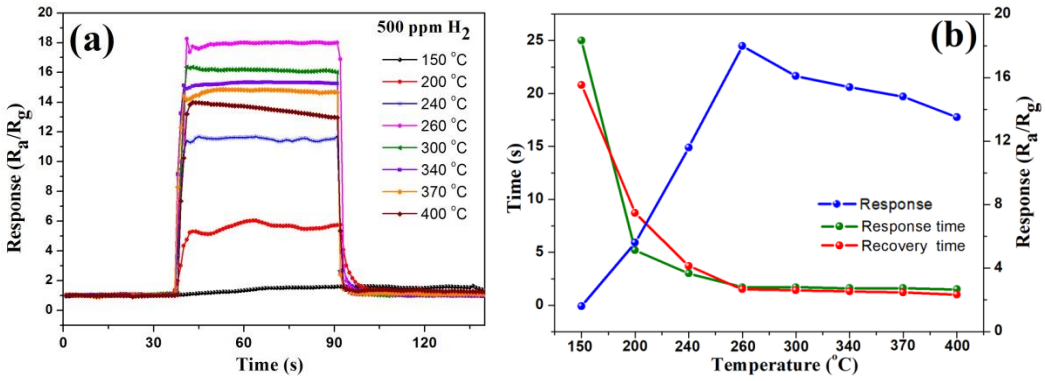

Fig. 5 (a) Response/recovery curves and (b) response values and response/recovery times of the mesoporous In_2O_3 based sensor to 500 ppm of hydrogen measured at different working temperatures from 150 °C to 400 °C.

The response and recovery of the mesoporous In_2O_3 based sensor towards hydrogen with a concentration of 500 ppm were measured at different working temperatures and the results are shown in Fig. 5. As can be seen from Fig. 5a, the sensor shows a stable baseline when measured in air. After it is exposed to hydrogen at a working temperature above 200 °C, the hydrogen molecules are absorbed and reacted with the oxygen species of O^- on the surfaces of In_2O_3 to release free electrons (see chemical reaction equation (5)) [36]. Generation of free electrons causes the decrease of the sensor's resistance. Because of the mesoporous structures and large specific surface area of the In_2O_3, and also lots of chemisorbed oxygen ions on its surfaces, the sensor exhibits fast response/recovery and a high response value to hydrogen, as shown in Fig. 5.

The calculated response values of the sensor are shown in Fig. 5b, and as defined before, the response is defined as the ratio between the resistance of the sensor in air (Ra) and that in the tested hydrogen (Rg). The response is increased with the increase of the temperature from 150 °C. It has a maximum value of 18.0 at 260 °C, at which

the adsorption and desorption of hydrogen molecules on the surfaces of In_2O_3 achieve an optimum balance and the reduction reaction with chemisorbed oxygen species reaches its maximum. Above 260 °C, the desorption of hydrogen becomes dominant due to the high temperature, thus resulting in a decrease of the reduction reaction of hydrogen molecules with chemisorbed oxygen species. Therefore, the response values are decreased at temperatures above 260 °C.

Fig. 5b also shows the response times (e.g., the time to reach 90% of the maximum response) and recovery times (e.g., the time to reach 10% of the response) of the sensor to 500 ppm of hydrogen at different working temperatures. Clearly, both the response times and recovery times are decreased significantly with the increase of the working temperature. At a working temperature above 260 °C, these values are all less than 2 s. Therefore, based on the above results, the optimum working temperature for this hydrogen gas sensor is 260 °C. In the following work, the sensing properties of this sensor were investigated at the working temperature of 260 °C.

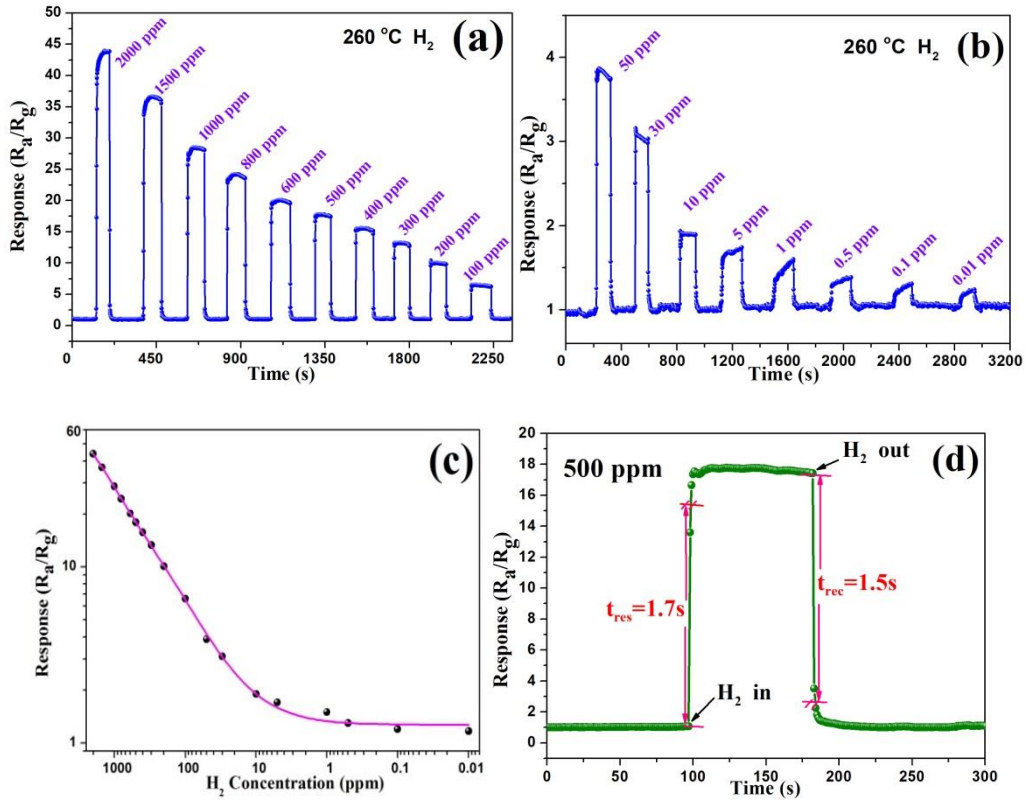

Fig. 6 (a, b)Response/recovery curves; (c) response values of the mesoporous In_2O_3 based sensor to different concentrations of hydrogen from 2000 ppm to 0.01 ppm at

260 ºC; (d) real-time gas sensing curve of the sensor to 500 ppm hydrogen at 260 ºC.

Fig. 6 shows the real-time sensing results of the mesoporous In_2O_3 based sensor exposed to different concentrations of hydrogen at 260 ºC. As shown in Figs. 6a and 6b, the sensor shows obvious responses to all concentrations of hydrogen with fast response/recovery behaviors and good reversibility. From Fig. 6c, the response values are strongly dependent on the concentration of hydrogen, e.g., they increase with the hydrogen concentration. Due to lots of chemisorbed oxygen ions adsorbed on the surfaces of mesoporous In_2O_3, the sensor shows high response values, e.g., with a value of 43.8 to 2000 ppm of hydrogen. For a low concentration of 0.01 ppm, the sensor sill shows an obvious response value of 1.2, indicating that the sensor has a low detection limit of 10 ppb.

It is well-known that fast response and recovery speeds are critical for the application of gas sensors [54]. Fig. 6d shows the real-time gas sensing curve of the mesoporous In_2O_3 based sensor to 500 ppm hydrogen at the working temperature of 260 ºC. The almost square shape of the response and recovery curves indicates that the sensor has fast response and recovery characteristics upon injection and extraction of hydrogen. Because the mesoporous structures of the In_2O_3 are beneficial to the adsorption and desorption of hydrogen, the sensor shows fast response and recovery speeds. Based on Fig. 6d, the obtained response and recovery times are 1.7 s and 1.5 s respectively, which are the lowest reported values if compared to those sensors based on different metal oxides listed in Table 1. Therefore, the sensor exhibits very fast response and recovery speeds for the hydrogen detection.

Compared with other hydrogen gas sensors based on pure metal oxides in the literature [31, 32] listed in Table 1, the hydrogen gas sensor in this study shows not only faster response/recovery times, but also a lower detection limit. Although the hydrogen sensors based on TiO_2 thin film [26] and CuO nanowire networks [29] showed faster response values compared with this study, their response times were reported to be 120 s and 60 s, respectively, which are much longer than what the mesoporous In_2O_3 based sensor has achieved in this study. Hydrogen gas sensor based

on the MoO_3 nanowires [27] also showed fast response and recovery times of 3.0 s and 2.7 s, respectively, but its response value was only 0.85 ($(R_{air}-R_{H2})/R_{H2}$) to 15000 ppm of hydrogen, and its reported detection limit was 100 ppm. Clearly the mesoporous In_2O_3 based sensor fabricated in this study shows much better sensing performance for hydrogen detection, which is mainly attributed to the formation of mesoporous structures, the large specific surface areas and numerous chemisorbed oxygen ions on the surfaces of the mesoporous In_2O_3.

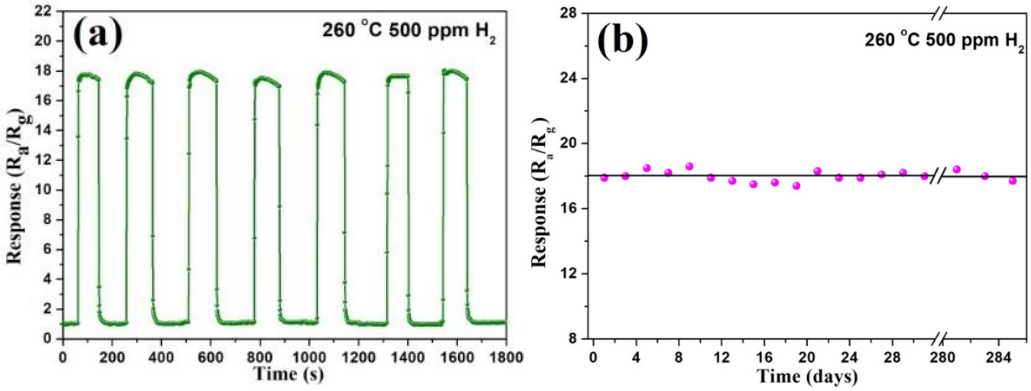

Fig. 7 (a) Reproducibility and (b) stability of the sensor based on mesoporous In_2O_3 for 500 ppm of hydrogen at 260 °C.

The reproducibility of the mesoporous In_2O_3 based sensor was tested by successively exposing the sensor to 500 ppm of hydrogen for sequential seven cycles. Fig. 7a shows the corresponding response/recovery curves. It can be seen that the response/recovery characteristics were repeated in the seven tested cycles, meaning that the sensor exhibits a good reproducibility for hydrogen detection. The stability of the hydrogen gas sensor was also tested by continuously measuring the response of the devices within a month period and the results are shown in Fig. 7b. The sensor shows an almost constant responses with a maximum deviation below 3% during one month period. Furthermore, this sensor was tested after 280 days, and still showed stable response values as shown in Fig. 7b. Therefore, it is clear that the hydrogen gas sensors based on the mesoporous In_2O_3 have excellent reproducibility and stability.

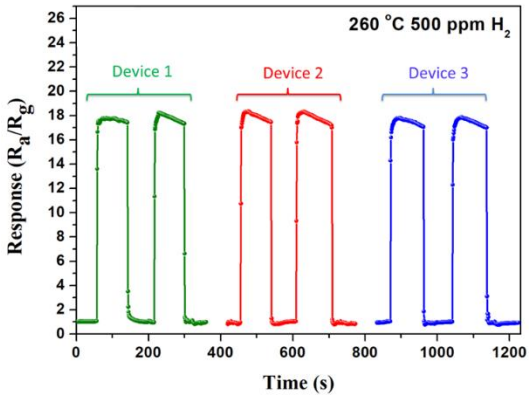

Fig. 8 Performance repeatability among three sensor devices based on mesoporous In_2O_3.

To verify the performance repeatability among different batches of sensors, three gas sensing devices based on the mesoporous In_2O_3 were fabricated and their sensing performance was evaluated. The response/recovery curves for 500 ppm of hydrogen at 260 °C are shown in Fig. 8. It can be clearly seen that the three sensor devices show similar response/recovery curves to hydrogen gas, which proves the good performance of repeatability for the mesoporous In_2O_3 based sensors.

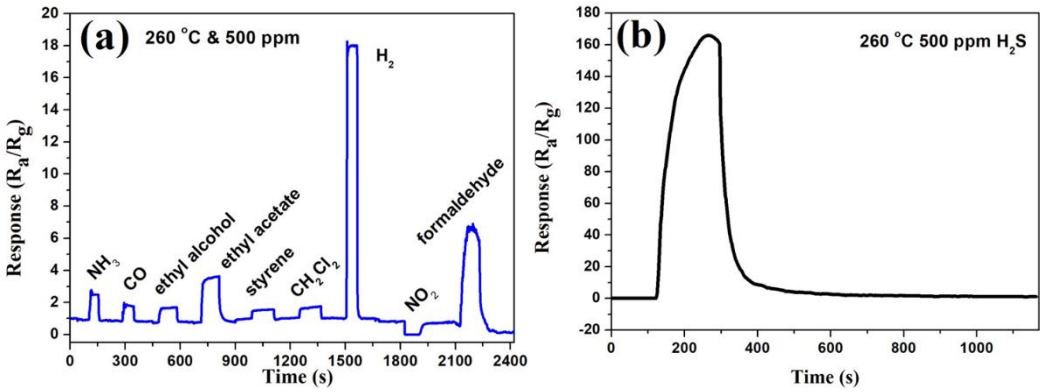

Fig. 9 Response/recovery curves of the mesoporous In_2O_3 based sensor to different gases with a concentration of 500 ppm at 260 °C: (a) NH_3, CO, ethyl alcohol, ethyl acetate, styrene, CH_2Cl_2, NO_2 and formaldehyde, and (b) H_2S.

The good selectivity is important for hydrogen detection to avoid the interference by other gases [55]. Therefore, the responses of this mesoporous In_2O_3 based sensor to other types of gases (including NH_3, CO, ethyl alcohol, ethyl acetate, styrene, CH_2Cl_2, NO_2, formaldehyde and H_2S) at a fixed concentration of 500 ppm were measured at 260 °C. Fig. 9 shows the response/recovery curves of the mesoporous

In_2O_3 based sensor to the different types of gases. It can be seen that the response of the sensor to H_2S is much higher than that to hydrogen. However, the responses of the sensor to other types of gases such as NH_3, CO, ethyl alcohol, ethyl acetate, styrene, CH_2Cl_2 and formaldehyde are much lower than that to hydrogen. A special case is for NO_2, which is oxidizing gas. The resistance of the sensor increases when the sensor is exposed to NO_2 gas, which is the opposite with that to the hydrogen. Therefore, except for H_2S, the mesoporous In_2O_3 based sensor has a very good selectivity to all the other tested gases. It was also found that after finishing sensing of any one of these gases, the response/recovery curves of this sensor showed good reversible and stable sensing performance when it was immediately exposed to hydrogen, without showing any poisonous effect to the sensor.

4. Conclusions

Mesoporous In_2O_3 was prepared using facile hydrothermal reaction and calcination processes. TEM analysis and nitrogen adsorption-desorption isotherm demonstrated that the synthesized In_2O_3 had lot of mesoporous and large specific surface areas, and XPS analysis proved that there were numerous chemisorbed oxygen ions on the surfaces of mesoporous In_2O_3. The hydrogen sensor made of mesoporous In_2O_3 showed not only high response values, but also fast response/recovery (e.g. 1.7 s/1.5 s for 500 ppm of hydrogen) and a detection limit of 0.01 ppm at an optimum working temperature of 260 ^oC. The sensor showed good reversibility, reproducibility and long-term stability in H_2 gas detection. Therefore, the fast response/recovery, high selectivity and sensitivity and ppb level detection limit demonstrated that the sensor based on the mesoporous In_2O_3 is promising for hydrogen detection. Because the optimum working temperature of the hydrogen sensor based on mesoporous In_2O_3 is 260 ^oC, the potential problem for the successful application of this technology is that heating is needed during the sensing process. Therefore, if the hydrogen concentration is greater than the lower flammable limit of H_2 (40,000 ppm), isolation of the heating source with the hydrogen gas becomes critical, which needs some special designs. In the future work, we will further explore

the different ways for the isolation of the heating source and measurement unit.

Acknowledgments

This work was supported by the Funding supports from UK Engineering Physics and Science Research Council (EPSRC EP/P018998/1), Newton Mobility Grant (IE161019) through Royal Society and NFSC, and Royal academy of Engineering UK-Research Exchange with China and India are also acknowledged.

References

[1] Fahad HM, Gupta N, Han R, Desai SB, Javey A. Highly Sensitive Bulk Silicon Chemical Sensors with Sub-5 nm Thin Charge Inversion Layers. ACS Nano 2018;12:2948-2954.

[2] Pang YK, Chen LB, Hu GJ, Luo JJ, Yang ZW, Zhang C, Wang ZL. Tribotronic transistor sensor for enhanced hydrogen detection. Nano Res 2017;10:3857-3864.

[3] Kim S, Song Y, Lim HR, Kwon YT, Hwang TY, Song E, Lee S, Lee YI , Cho HB, Choa YH. Fabrication and characterization of thermochemical hydrogen sensor with laminated structure. Int J Hydrogen Energy 2017;42:749-756.

[4] Kim S, Lee YI, Choi YM, Lim HR, Lim JH, Myung NV, Choa YH. Thermochemical hydrogen sensor based on chalcogenide nanowire arrays. Nanotechnology 2015;26:145503.

[5] Jang JS, Qiao S, Cho SJ, Jha G, Ogata AF, Koo WT, Kim DH, Kim ID, Penner RM. Hollow Pd-Ag composite nanowires for fast responding and transparent hydrogen sensors. ACS Appl Mater Interfaces 2017;9:39464-39474.

[6] Wu B, Zhao C, Xu B, Li Y. Optical fiber hydrogen sensor with single Sagnac interferometer loop based on vernier effect. Sens Actuators B Chem 2018;255:3011-3016.

[7] Zhang Y-n, Peng H, Qian X, Zhang Y, An G, Zhao Y. Recent advancements in optical fiber hydrogen sensors. Sens Actuators B Chem 2017;244:393-416.

[8] Dai JX, Peng W, Wang GP, Xiang F, Qin YH, Wang M, Yang MH, Deng H, Zhang PC. Improved performance of fiber optic hydrogen sensor based on WO_3-Pd_2Pt-Pt composite film and self-referenced demodulation method. Sens Actuators B Chem 2017;249:210-216.

[9] Perez-Cortes L, Hernandez-Rodriguez C, Mazingue T, Lomello-Tafin M. Functionality of Surface Acoustic Wave (SAW) transducer for palladium-platinum-based hydrogen sensor. Sensor Actuat A-Phys 2016;251:35-41.

[10] Viespe C, Miu D. Surface acoustic wave sensor with Pd/ZnO bilayer structure for room temperature hydrogen detection. Sensors 2017;17:1529.

[11] Amani E, Khojier K, Zoriasatain S. Improving the hydrogen gas sensitivity of WO_3 thin films by modifying the deposition angle and thickness of different promoter layers. Int J Hydrogen Energy 2017;42:29620-29628.

[12] Rahmani MB, Yaacob MH, Sabri YM. Hydrogen sensors based on 2D WO_3 nanosheets prepared by anodization. Sens Actuators B Chem 2017;251:57-64.

[13] Choi SJ, Chattopadhyay S, Kim JJ, Kim SJ, Tuller HL, Rutledge GC, Kim ID. Coaxial electrospinning of WO_3 nanotubes functionalized with bio-inspired Pd catalysts and their superior hydrogen sensing performance. Nanoscale 2016;8:9159-9166.

[14] Fardindoost S, Zad AI, Hosseini ZS, Hatamie S. Detecting hydrogen using graphene quantum

dots/WO_3 thin films. Mater Res Express 2016;3:116407.
[15] Mohammad SM, Hassan Z, Talib RA, Ahmed NM, Al-Azawi MA, Abd-Alghafour NM, Chin CW, Al-Hardan NH. Fabrication of a highly flexible low-cost H_2 gas sensor using ZnO nanorods grown on an ultra-thin nylon substrate. J Mater Sci-Mater El 2016;27:9461-9469.
[16] Ranwa S, Barala SS, Fanetti M, Kumar M. Effect of gamma irradiation on Schottky-contacted vertically aligned ZnO nanorod-based hydrogen sensor. Nanotechnology 2016;27:345502.
[17] Ranwa S, Kumar M, Singh J, Fanetti M, Kumar M. Schottky-contacted vertically self-aligned ZnO nanorods for hydrogen gas nanosensor applications. J Appl Phys 2015;118:034509.
[18] Hassan JJ, Mahdi MA, Chin CW, Abu-Hassan H, Hassan Z. Room temperature hydrogen gas sensor based on ZnO nanorod arrays grown on a SiO_2/Si substrate via a microwave-assisted chemical solution method. J Alloy Compd 2013;546:107-111.
[19] Abubakar D, Ahmed NM, Mahmud S, Algadri NA. Properties of NiO nanostructured growth using thermal dry oxidation of nickel metal thin film for hydrogen gas sensing at room temperature. Mater Res Express 2017;4:075009.
[20] Thi Thanh Le D, Tonezzer M, Van Hieu N. Hydrothermal growth and hydrogen selective sensing of nickel oxide nanowires. J Nanomater 2015:785856.
[21] Soleimanpour AM, Khare SV, Jayatissa AH. Enhancement of hydrogen gas sensing of nanocrystalline nickel oxide by pulsed-laser Irradiation. ACS Appl Mater Interfaces 2012;4:4651-4657.
[22] Nguyen VT, Nguyen VC, Nguyen VD, Hoang SH, Hugo N, Nguyen DH, Nguyen VH. Fabrication of highly sensitive and selective H□ gas sensor based on SnO□ thin film sensitized with microsized Pd islands. J Hazard Mater 2016;301:433-442.
[23] Ab Kadir R, Li Z, Sadek AZ, Rani RA, Zoolfakar AS, Field MR, Ou JZ, Chrimes AF, Kalantar-zadeh K. Electrospun granular hollow SnO_2 nanofibers hydrogen gas sensors operating at low temperatures. J Phys Chem C 2014;118:3129-3139.
[24] Liu L, Liu CB, Li SC, Wang LY, Shan H, Zhang XB, Guan HY, Liu Z. Honeycombed SnO_2 with ultra sensitive properties to H_2. Sens Actuators B Chem 2013;177:893-897.
[25] Hazra A, Das S, Kanungo J, Sarkar CK, Basu S. Studies on a resistive gas sensor based on sol-gel grown nanocrystalline p-TiO_2 thin film for fast hydrogen detection. Sens Actuators B Chem 2013;183:87-95.
[26] Haidry AA, Puskelova J, Plecenik T, Durina P, Gregus J, Truchly M, et al. Characterization and hydrogen gas sensing properties of TiO_2 thin films prepared by sol-gel method. Appl Surf Sci 2012;259:270-275.
[27] Luo XT, You KK, Hu YM, Yang SL, Pan XM, Wang Z, Chen WP, Gu HS. Rapid hydrogen sensing response and aging of alpha-MoO_3 nanowires paper sensor. Int J Hydrogen Energy 2017;42:8399-8405.
[28] Kalanur SS, Yoo IH, Seo H. Pd on MoO_3 nanoplates as small-polaron-resonant eye-readable gasochromic and electrical hydrogen sensor. Sens Actuators B Chem 2017;247:357-365.
[29] Lupan O, Postica V, Ababii N, Hoppe M, Cretu V, Tiginyanu I, Sontea V, Pauporte T, Viana B, Adelung R. Influence of CuO nanostructures morphology on hydrogen gas sensing performances. Microelectron Eng 2016;164:63-70.
[30] Pradeep N, Venkatachalaiah C, Venkatraman U, Santhosh C, Bhatnagar A, Jeong SK, Grace AN. Magnesium oxide nanocubes deposited on an overhead projector sheet: synthesis and resistivity-based hydrogen sensing capability. Microchim Acta 2017;184:3349-3355.
[31] Chen L, He X, Liang Y, Sun Y, Zhao Z, Hu J. Synthesis and gas sensing properties of palladium-doped indium oxide microstructures for enhanced hydrogen detection. J Mater Sci-Mater El

2016;27:11331-11338.
[32] Qurashi A, El-Maghraby EM, Yamazaki T, Kikuta T. Catalyst supported growth of In_2O_3 nanostructures and their hydrogen gas sensing properties. Sens Actuators B Chem 2010;147:48-54.
[33] Chu J, Peng X, Wang Z, Feng P. Sensing performances of ZnO nanostructures grown under different oxygen pressures to hydrogen. Mater Res Bull 2012;47:4420-4426.
[34] Kathiravan D, Huang BR, Saravanan A. Self-Assembled hierarchical interfaces of ZnO nanotubes/graphene heterostructures for efficient room temperature hydrogen sensors. ACS Appl Mater Interfaces 2017;9:12064-12072.
[35] Huang Y, Chen W, Zhang S, Kuang Z, Ao D, Alkurd NR, et al. A high performance hydrogen sulfide gas sensor based on porous α-Fe_2O_3 operates at room-temperature. Appl Surf Sci 2015;351:1025-1033.
[36] Fan H, Xu SC, Cao XM, Liu DX, Yin YY, Hao HY, Wei DZ, Shen YB. Ultra-long Zn_2SnO_4-ZnO microwires based gas sensor for hydrogen detection. Appl Surf Sci 2017;400:440-445.
[37] Wang Y, Zhao ZT, Sun YJ, Li PW, Ji JL, Chen Y, Zhang WD, Hu J. Fabrication and gas sensing properties of Au-loaded SnO_2 composite nanoparticles for highly sensitive hydrogen detection. Sens Actuators B Chem 2017;240:664-673.
[38] Li YX, Deng DY, Chen N, Xing XX, Liu X, Xiao XC, Wang YD. Pd nanoparticles composited SnO_2 microspheres as sensing materials for gas sensors with enhanced hydrogen response performances. J Alloy Compd 2017;710:216-224.
[39] Lupan O, Postica V, Labat F, Ciofini I, Pauporte T, Adelung R. Ultra-sensitive and selective hydrogen nanosensor with fast response at room temperature based on a single Pd/ZnO nanowire. Sens Actuators B Chem 2018;254:1259-1270.
[40] Wang YR, Liu B, Cai DP, Li H, Liu Y, Wang DD, Wang LL, Li QH, Wang TH. Room-temperature hydrogen sensor based on grain-boundary controlled Pt decorated In_2O_3 nanocubes. Sens Actuators B Chem 2014;201:351-359.
[41] Navale ST, Liu C, Yang Z, Patil VB, Cao P, Du B, Mane RS, Stadler FJ. Low-temperature wet chemical synthesis strategy of In_2O_3 for selective detection of NO2 down to ppb levels J Alloy Compd. 2018;735:2102-2110.
[42] Zhang SC, Huang YW, Kuang Z, Wang SY, Song WL, Ao DY, Liu W, Li ZJ. Solvothermal synthesized In_2O_3 nanoparticles for ppb level H_2S detection. Nanosci Nanotech Let 2015;7:455-461.
[43] Lim SK, Hwang S-H, Chang D, Kim S. Preparation of mesoporous In_2O_3 nanofibers by electrospinning and their application as a CO gas sensor. Sens Actuators B Chem 2010;149:28-33.
[44] Huang F, Yang W, He F, Liu S. Controlled synthesis of flower-like In_2O_3 microrods and their highly improved selectivity toward ethanol. Sens Actuators B Chem 2016;235:86-93.
[45] Gu F, Li C, Han D, Wang Z. Manipulating the defect structure (V-O) of In_2O_3 nanoparticles for enhancement of formaldehyde detection. ACS Appl Mater Interfaces 2018;10:933-942.
[46] Li Z, Wang N, Lin Z, Wang J, Liu W, Sun K, Fu YQ, Wang ZG. Room-temperature high-performance H_2S sensor based on porous CuO nanosheets prepared by hydrothermal method. ACS Appl Mater Interfaces 2016;8:20962-20968.
[47] Gao J, Wu HY, Zhou J, Yao LY, Zhang G, Xu S, Xie Y, Li L, Shi KY. Mesoporous In_2O_3 nanocrystals: synthesis, characterization and NO_x gas sensor at room temperature. New J Chem 2016;40:1306-13011.
[48] Ullah H, Khan I, Yamani ZH, Qurashi A. Sonochemical-driven ultrafast facile synthesis of SnO_2 nanoparticles: Growth mechanism structural electrical and hydrogen gas sensing properties. Ultrason

Sonochem 2017;34:484-490.
[49] Cho I, Kang K, Yang D, Yun J, Park I. Localized liquid-phase synthesis of porous SnO_2 nanotubes on MEMS platform for low-power, high performance gas sensors. ACS Appl Mater Interfaces 2017;9:27111-27119.
[50] Wang JQ, Li ZJ, Zhang S, Yan S, Cao BB, Wang ZG, Fu YQ. Enhanced NH_3 gas-sensing performance of silica modified CeO_2 nanostructure based sensors. Sens Actuators B Chem 2018;255:862-870.
[51] Fan H, Shen W. Gelatin-Based Microporous Carbon Nanosheets as High Performance Supercapacitor Electrodes. Acs Sustain Chem Eng 2016;4:1328-1337.
[52] Geng Q, Karkyngul B, Sun C, Liang X, Yang C, Su X. In_2O_3 nanocubes derived from monodisperse InOOH nanocubes: synthesis and applications in gas sensors. J Mater Sci 2017;52:5097-5105.
[53] Liu JJ, Chen G, Yu YG, Wu YL, Zhou MJ, Zhang HQ, Lv CD, Qin H, Qi X. Template-free preparation of mesoporous single crystal In_2O_3 achieving superior ethanol gas sensing performance. RSC Adv 2016;6:14615-14619.
[54] Boon-Brett L, Black G, Moretto P, Bousek J. A comparison of test methods for the measurement of hydrogen sensor response and recovery times. Int J Hydrogen Energy 2010;35:7652-7663.
[55] Ren S, Fan G, Qu S, Wang Q. Enhanced H_2 sensitivity at room temperature of ZnO nanowires functionalized by Pd nanoparticles. J Appl Phys 2011;110:084312.